Cell cycle–regulated cortical dynein/dynactin promotes symmetric cell division by differential pole motion in anaphase

Elizabeth S. Collins[a], Sai Keshavan Balchand[a,b], Jessica L. Faraci[a], Patricia Wadsworth[a,b], and Wei-Lih Lee[a,b]

[a]Biology Department and [b]Molecular and Cellular Biology Program, University of Massachusetts, Amherst, MA 01003

ABSTRACT **In cultured mammalian cells, how dynein/dynactin contributes to spindle positioning is poorly understood. To assess the role of cortical dynein/dynactin in this process, we generated mammalian cell lines expressing localization and affinity purification (LAP)–tagged dynein/dynactin subunits from bacterial artificial chromosomes and observed asymmetric cortical localization of dynein and dynactin during mitosis. In cells with asymmetrically positioned spindles, dynein and dynactin were both enriched at the cortex distal to the spindle. NuMA, an upstream targeting factor, localized asymmetrically along the cell cortex in a manner similar to dynein and dynactin. During spindle motion toward the distal cortex, dynein and dynactin were locally diminished and subsequently enriched at the new distal cortex. At anaphase onset, we observed a transient increase in cortical dynein, followed by a reduction in telophase. Spindle motion frequently resulted in cells entering anaphase with an asymmetrically positioned spindle. These cells gave rise to symmetric daughter cells by dynein-dependent differential spindle pole motion in anaphase. Our results demonstrate that cortical dynein and dynactin dynamically associate with the cell cortex in a cell cycle–regulated manner and are required to correct spindle mispositioning in LLC-Pk1 epithelial cells.**

Monitoring Editor
Erika Holzbaur
University of Pennsylvania

Received: Feb 13, 2012
Revised: Jul 5, 2012
Accepted: Jul 13, 2012

INTRODUCTION

The position of the mitotic spindle dictates the location of cytokinesis in diverse cells, thus regulating the size of the two daughter cells (Rappaport, 1996). Although most somatic cells divide symmetrically to generate two equivalent daughter cells, asymmetric cell division is an important process for cell fate determination and morphogenesis during development (Gillies and Cabernard, 2011; Morin and Bellaiche, 2011; Siller and Doe, 2009). In both symmetric and asymmetric divisions, spindle positioning is accomplished by the interactions of dynamic astral microtubules with cytoplasmic or cortical force generators (FGs; Carminati and Stearns, 1997; Dujardin and Vallee, 2002; McCarthy and Goldstein, 2006; Markus *et al.*, 2009; Markus and Lee, 2011; Wuhr *et al.*, 2010; Kimura and Kimura, 2011). Intrinsic signals, such as cortical marks, or extrinsic cues, such as signaling from neighboring cells, influence these interactions by regulating the recruitment or activation of FGs in a spatial and temporal manner, thereby controlling spindle placement in the dividing cell (Morrison and Kimble, 2006; Knoblich, 2010).

A particularly well-studied example of asymmetric spindle positioning is the first mitotic division in the *Caenorhabditis elegans* embryo, in which the spindle moves toward, and is maintained at, the posterior cortex, giving rise to a larger anterior and a smaller posterior cell (Cowan and Hyman, 2004; Nguyen-Ngoc *et al.*, 2007). Laser ablation experiments show that FGs are present along the cortex of the embryo, with higher FG activity at the posterior cortex resulting in a larger net pulling force acting on the posterior spindle pole (Grill *et al.*, 2001, 2003; Labbe *et al.*, 2004; Krueger *et al.*, 2010). FGs at the posterior cortex also contribute to the characteristic spindle rocking and flattening of the posterior pole observed during movements of the pole toward the posterior cortex (Schneider and Bowerman, 2003). The minus end–directed microtubule motor

This article was published online ahead of print in MBoC in Press (http://www.molbiolcell.org/cgi/doi/10.1091/mbc.E12-02-0109) on July 18, 2012.

Address correspondence to: Wei-Lih Lee (wlee@bio.umass.edu).

Abbreviations used: BAC, bacterial artificial chromosome; DHC, dynein heavy chain; FG, force generator; LAP, localization and affinity purification; MDCK, Madin–Darby canine kidney; NRK, normal rat kidney.

cytoplasmic dynein has been a prime candidate for the cortical FG. However, the mechanism by which dynein generates asymmetric force during metaphase/anaphase is unclear, as components of the dynein complex are not enriched at the posterior cortex of the *C. elegans* embryo (Couwenbergs *et al.*, 2007; Nguyen-Ngoc *et al.*, 2007). Similarly, during asymmetric divisions of *Drosophila* neuroblast cells, dynein is believed to exert force to orient the mitotic spindle along the apical–basal cell axis, but the dynein complex, and its regulator dynactin, are not enriched at the neuroblast apical cortex (Siller *et al.*, 2005; Siller and Doe, 2008).

Emerging data suggest that a highly conserved pathway regulates recruitment of dynein and dynactin to the cell cortex for asymmetric spindle positioning. This pathway consists of the noncanonical Gαi protein, which interacts with LGN (Du and Macara, 2004). LGN can simultaneously interact with Gαi at the membrane and with NuMA, a microtubule-associated protein originally identified for its contribution to spindle pole formation (Merdes *et al.*, 1996). NuMA can bind microtubules and has been shown to form a complex with dynein and dynactin (Merdes *et al.*, 1996). Because NuMA cannot bind LGN and microtubules simultaneously due to overlapping binding sites (Du *et al.*, 2002), a favored hypothesis is that NuMA tethers the spindle by transiently associating with astral microtubules and by promoting dynein and dynactin recruitment to the cortical sites. In addition, overexpression of either Gαi or LGN in mammalian cells results in spindle rocking (Du and Macara, 2004), reminiscent of spindle behavior in *C. elegans*.

In contrast to the well-studied asymmetric cell divisions that occur in worms and flies, most mammalian cells in culture divide symmetrically: the mitotic spindle is positioned at or near the geometric center of the cell, parallel to the substrate (O'Connell and Wang, 2000). Micromanipulation experiments show that normal rat kidney (NRK) cells contain a sensory mechanism that continuously monitors spindle position and maintains spindle orientation with respect to the long axis of the cell (O'Connell and Wang, 2000). Dynein/dynactin appears to be required for this surveillance mechanism and has been localized by immunofluorescence to the cell cortex and the plus ends of astral microtubules (Busson *et al.*, 1998; Faulkner *et al.*, 2000; O'Connell and Wang, 2000; Kobayashi and Murayama, 2009). Accordingly, treatments that alter astral microtubule dynamics, misregulate dynein, or reduce end-on contacts of astral microtubules with the cortex have been shown to result in spindles that are no longer positioned at the cell center (Faulkner *et al.*, 2000; O'Connell and Wang, 2000; Rankin and Wordeman, 2010; Bruning-Richardson *et al.*, 2011; Samora *et al.*, 2011).

Our previous work in LLC-Pk1 cells showed that microtubule fragments released from the spindle pole during anaphase are transported along the cell cortex, with the plus ends leading; in metaphase cells, however, release and transport of microtubules was rarely observed (Rusan and Wadsworth, 2005). These data suggest the existence of cortically localized, minus end–directed motor proteins and further demonstrate that the localization and/or activity of these motors are regulated by the cell cycle. In the study described here, we found that dynein, dynactin, and the upstream targeting factor NuMA are asymmetrically localized to the cell cortex of mitotic cells, consistent with recent work in HeLa cells (Kiyomitsu and Cheeseman, 2012). We provide evidence that cortical dynein and dynactin are regulated by astral microtubules, polo kinase (Plk1) activity, and the cell cycle. Spindles in LLC-Pk1 cells frequently move along the long axis of the cell, and many cells enter anaphase with an asymmetrically positioned spindle. Of interest, cells with asymmetrically positioned spindles generate symmetric daughter cells via a dynein-dependent differential spindle pole motion during anaphase.

RESULTS

Asymmetric distribution of dynein and dynactin at the cortex in mitotic LLC-Pk1 cells

To gain insight into how dynein and dynactin contribute to spindle positioning in mammalian cells, we generated clonal cell lines expressing localization and affinity purification (LAP)–tagged proteins from bacterial artificial chromosomes (BACs; Cheeseman and Desai, 2005; Poser *et al.*, 2008). With this approach the native regulatory elements are present, and the gene of interest is expressed from the endogenous promoter. For the experiments reported here we used two cell lines, one expressing LAP-tagged dynein heavy chain (DHC) and the other expressing LAP-tagged p50 subunit of dynactin; we refer to the tagged DHC and p50 as dynein and dynactin, respectively. Using the S-tag (in LAP) to retrieve proteins from mitotic cell lysates, we confirmed that dynein and dynactin subunits expressed from BACs were present in native complexes that could interact (Supplemental Figure S1, A–C), consistent with prior results (Poser *et al.*, 2008). Spindle length and mitotic index were similar to those of parental cells (Supplemental Figure S1, D and E), and no abnormalities in mitosis were detected (unpublished data). In addition, because overexpression of p50 is known to disrupt dynactin integrity (Echeverri *et al.*, 1996; Burkhardt *et al.*, 1997; LaMonte *et al.*, 2002), we selected a cell line that exhibited a lower expression level than the endogenous p50 for the following studies (Supplemental Figure S1F).

In mitotic LLC-Pk1 epithelial cells, dynein and dynactin were observed at centrosomes, along spindle microtubules, at kinetochores, and at the cell cortex, consistent with previous reports and supporting the functionality of the BAC approach used here (Figure 1, A and B; Busson *et al.*, 1998; Faulkner *et al.*, 2000; Kobayashi and Murayama, 2009; Ligon *et al.*, 2001; Woodard *et al.*, 2010; Kiyomitsu and Cheeseman, 2012). By total internal reflection fluorescence microscopy, we observed DHC and p50 at the microtubule plus ends with rates consistent with tip tracking (Supplemental Figure S1G). We did not detect any differences in the distribution of dynein and dynactin throughout mitosis (Figure 1, C and D).

We next focused on cortical dynein and dynactin and their role in spindle positioning. In prometaphase and metaphase cells with centrally positioned spindles (symmetrically near the cell center), dynein and dynactin were either absent from the cortex (Figure 1, C and D) or were observed at each end of the cell in a crescent-shaped distribution (Figure 1A, top, C and D, and Supplemental Movies S1 and S2). Cortical dynein and dynactin were not detected at the equatorial region. In cells with asymmetrically positioned spindles, bright patches of dynein and dynactin were observed at the cortex furthest from the spindle (Figure 1, A and B, bottom rows, and Supplemental Movies S3–S5). Time-lapse imaging showed that the distribution of cortical dynein and dynactin changed as the metaphase spindle moved within the cell, as reported previously (Kiyomitsu and Cheeseman, 2012). In the example shown in Figure 1B (top), cortical patches of dynactin were detected at regions distal to the spindle at 0 min. Their fluorescence diminished as the spindle moved toward them at 21 min; new patches subsequently appeared at the new distal cortex after the spindle movement (red arrowheads at 21 min). These results demonstrate that during metaphase the level of cortical dynein and dynactin changes, depending on the proximity of the spindle.

At anaphase onset, we noted that the intensity of cortical dynein and dynactin increased and subsequently decreased as cells progressed into cytokinesis (Supplemental Movies S1–S5). At anaphase, cortical dynein and dynactin appeared relatively smooth and uniform along the polar cortex and, similar to metaphase, were not

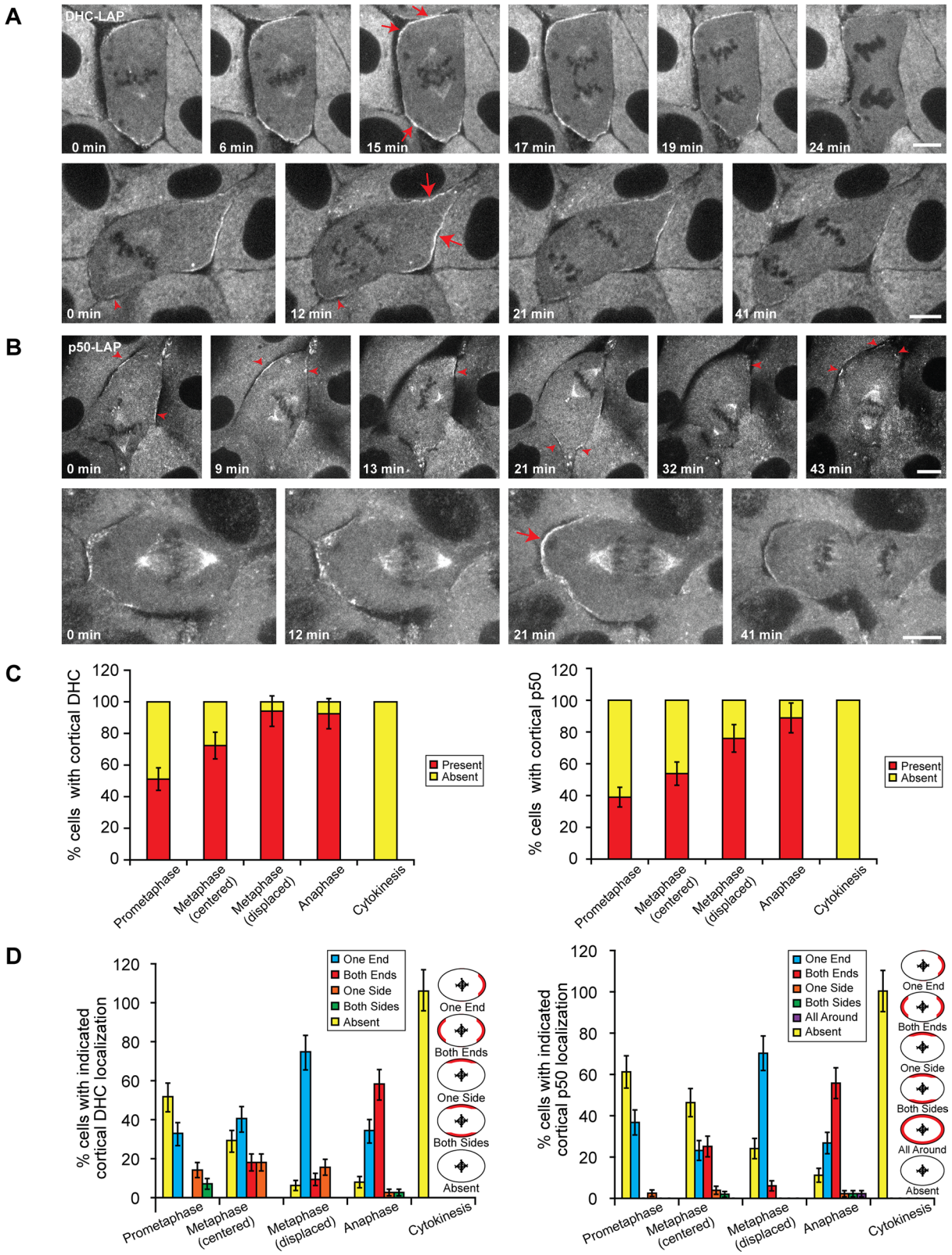

FIGURE 1: Dynamics of dynein and dynactin at the mitotic cortex of LLC-Pk1 cells. Time-lapse images of mitotic LLC-Pk1 cells expressing (A) DHC-LAP and (B) p50-LAP. (A) Top, a cell with centrally positioned spindle. Bottom, a cell with displaced mitotic spindle. (B) Top, a metaphase spindle becoming displaced before anaphase onset. Bottom, a cell with displaced mitotic spindle. Arrowheads, DHC-LAP signal at the proximal cortex (A, bottom) or dynamic p50-LAP signal (B, top). Arrows, enriched and uniform DHC-LAP and p50-LAP signal. Scale bars, 10 μm. (C, D) Quantitation of cortical dynein and dynactin localization throughout mitosis. (C) Percentage of cells exhibiting cortical dynactin and dynein localization. (D) Percentage of cells with indicated localization of cortical dynactin and dynein localization. Error bars in C and D represent SE of proportion; $n = 167$ (dynein) and 194 (dynactin) cells.

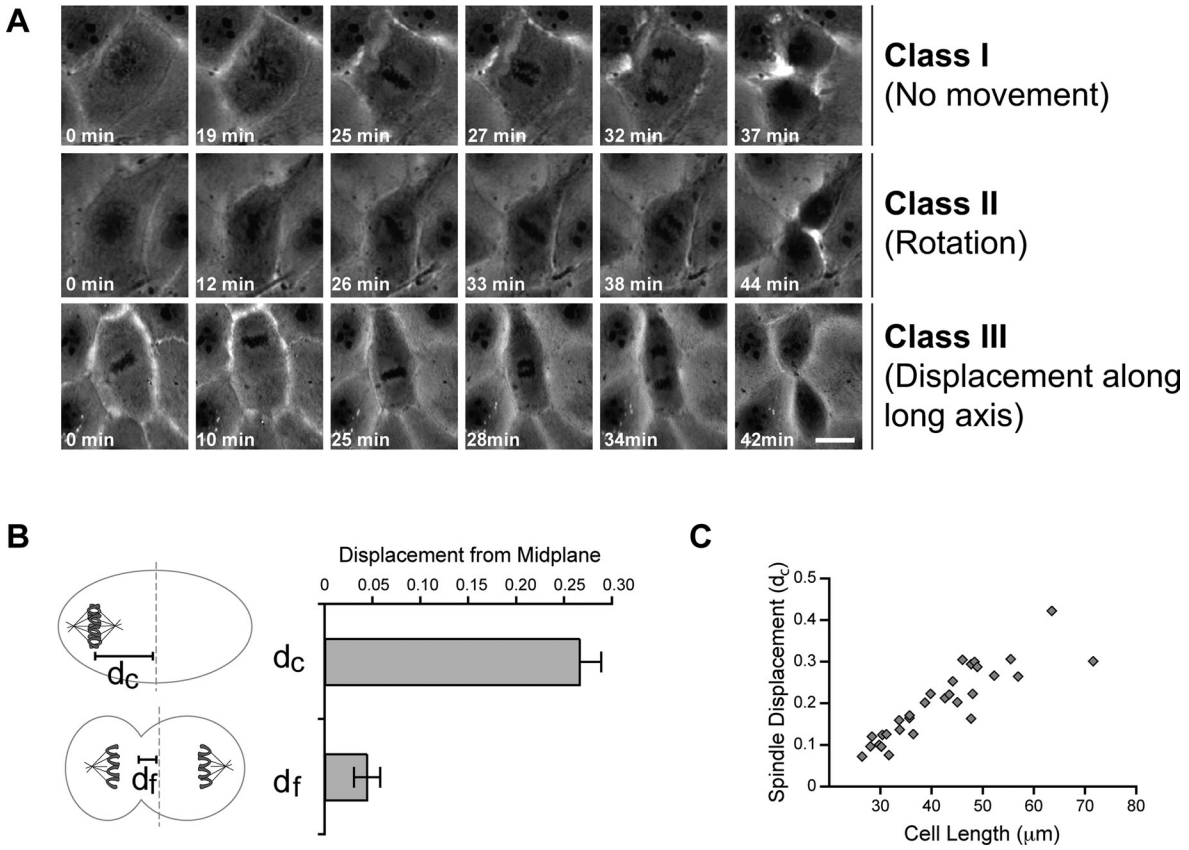

FIGURE 2: Classification of metaphase spindle movements in LLC-Pk1 cells. (A) Row 1, no spindle movement (class I). Row 2, rotational movement (class II). Row 3, displacement along long axis (class III). Scale bar, 10 μm. (B) Distance from the cell center to the chromosome plate measured at the last movie frame before anaphase (d_c) and to the cleavage furrow at cytokinesis (d_f; $p < 0.0001$). Error bars represent SE of proportion. (C) Relationship between cell length along the interpolar axis and the normalized displacement of the spindle at anaphase onset. For A–C, $n = 29$ cells; for B and C, all classes of LLC-Pk1 cells were included in the measurement.

detected at the equatorial region. For centrally located spindles, the observed increase in intensity occurred either at the onset of anaphase or as anaphase progressed (Figure 1A, top; compare 6 with 15 or 17 min, red arrows). For asymmetrically positioned spindles, the increase was more pronounced at the distal cortex (Figure 1, A and B, bottom, red arrows) but could sometimes be detected at the proximal cortex (Figure 1A, bottom, 12 min, arrowhead). The intensity of dynein and dynactin at the centrosome of neighboring interphase cells was unchanged throughout the image sequence (Supplemental Figure S2), indicating that the reduction in dynein or dynactin at the cortex in telophase was not due to photobleaching. These observations demonstrate that 1) cortical dynein and dynactin dynamically associate with the cell cortex, 2) during early mitosis, cortical dynein and dynactin are enriched in regions distal to the spindle and are diminished in regions near the spindle, and 3) the levels of cortical dynein and dynactin increase at anaphase onset and diminish as cells progress into cytokinesis.

LLC-Pk1 spindle movement parallel to the plane of the cell sheet

The observation that dynein and dynactin accumulate at the cortex distal to the spindle is counterintuitive: the prevailing view holds that dynein is required for spindle positioning, so one would expect a high concentration of dynein at the cortex proximal to the spindle. This observation led us to hypothesize that dynein/dynactin might be involved in a spindle position correction mechanism and that the levels of dynein/dynactin are reduced after interactions with astral microtubules.

To test this model, we performed time-lapse, phase contrast imaging of LLC-Pk1 cells from spindle assembly to cytokinesis (Figure 2A). The results showed that in 29% of metaphase cells, the spindle assembled at or near the geometric center of the cell (determined as the midpoint of the long axis of the cell) and remained in this location throughout mitosis. We call these cells class I. In 13% of imaged cells, spindle rotation was observed, resulting in the alignment of the spindle along the long axis of the cell, as previously observed for NRK cells (O'Connell and Wang, 2000). We call these cells class II. Strikingly, in 59% of recorded cells, the metaphase spindle was observed to move along the long axis of the cell and, in some cases, translocate from one end of the cell to the other. We call these class III. In these cells, the spindle was often located at one end of the cell at the onset of anaphase. The degree of spindle displacement at anaphase onset, measured as the distance of the spindle equator from the cell midplane (Figure 2B), was 0.27 ± 0.02 of the half-cell length. The extent of spindle displacement correlated with cell length (Figure 2C), indicating that longer cells have a greater tendency to enter anaphase with a mispositioned spindle. Nonetheless, we did not detect a delay in anaphase onset for class III LLC-Pk1 cells (unpublished data), suggesting that mitotic progression was not affected. Of interest, despite having a displaced spindle during metaphase, most class III cells proceeded through anaphase and cytokinesis to produce two daughter cells of equal size (the

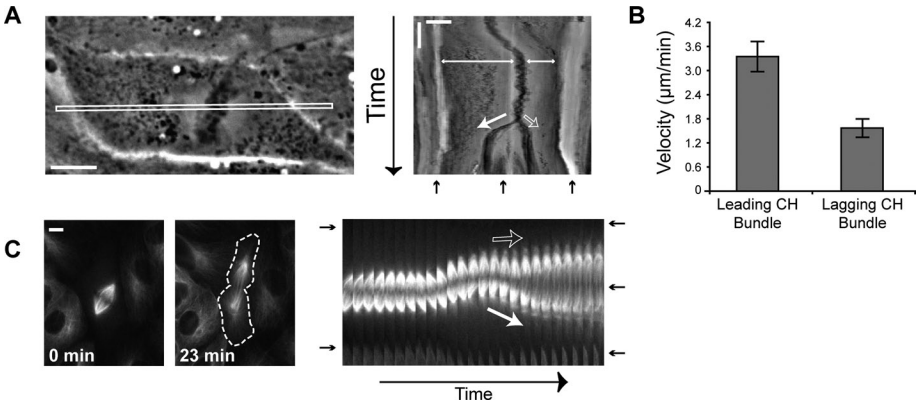

FIGURE 3: Asymmetric anaphase chromosome and pole movements result in symmetric division. (A) Phase contrast image of a cell with a displaced spindle (class III) at the start of time-lapse imaging and the corresponding kymograph of the boxed region. Scale bar, 10 μm (horizontal) and 10 min (vertical). (B) Average velocity of the leading and lagging chromosome bundles ($n = 9$ cells). Error bars, SE. (C) Differential pole movements during anaphase. GFP–α-tubulin images of a class III cell at $t = 0$ and 23 min and the corresponding kymograph. Dashed line outlines cell edge in the 23-min image. Scale bar, 10 μm. For A and C: closed white arrow, leading pole; open white arrow, lagging pole; double-headed arrow, spindle displacement; black arrow, cell edge and cleavage furrow.

ratio of the areas was 0.91 ± 0.03; $n = 18$), indicating that LLC-Pk1 cells possess a mechanism for correcting spindle displacement so as to generate equal-sized daughter cells.

Differential pole movements during anaphase correct spindle mispositioning

Recent work showed that anaphase spindle elongation can compensate for spindle displacement in mammalian cells (Xiao *et al.*, 2012). To determine how asymmetrically positioned metaphase spindles could result in symmetric cell divisions in LLC-Pk1 cells, we analyzed the movements of chromosomes and spindle poles during anaphase in class III cells (Figure 3A). We found that during anaphase, the two sets of chromosomes showed differential movement toward the opposite cell ends. Kymographs revealed that the leading set of chromosomes, defined as the chromosomes farthest from the cell cortex, moved a greater distance and at a twofold higher velocity than the lagging set of chromosomes (Figure 3B; 3.36 ± 0.36 vs. 1.56 ± 0.24 μm/min). Kymographs of class I cells showed that both sets of chromosomes moved the same distance at a similar rate (Supplemental Figure S3). The increased velocity of the leading set of chromosomes resulted in the correction of the spindle position without an apparent increase in the duration of anaphase (anaphase onset to furrow initiation was 11.5 ± 0.6 min for class III cells and 10.6 ± 0.6 min for class I cells).

To determine whether the differential movement of chromosomes was contributed by differential anaphase A (chromosome-to-pole) or anaphase B (pole–pole separation) motion, we examined class III cells expressing green fluorescent protein (GFP)–α-tubulin. Time-lapse images (Figure 3C) showed that, upon anaphase onset in a class III cell, the spindle elongated primarily due to the movement of one pole. The lagging pole (top pole in Figure 3C) remained relatively stationary, and the leading pole moved toward the opposite cell end. The lengths of the kinetochore fibers associated with the leading and lagging poles were equivalent throughout anaphase A, demonstrating that spindle pole motion in anaphase B is responsible for correcting the spindle displacement.

As a result of asymmetric spindle pole movements during spindle elongation, the spindle midzone and cleavage furrow formed near the geometric center of the cell. We found that the average displacement of the cleavage furrow from the cell center was significantly reduced from the average displacement of the spindle equator at metaphase (from 0.27 ± 0.02 to 0.04 ± 0.01; Figure 2B). These data show that differential anaphase spindle pole motions result in symmetric divisions in class III LLC-Pk1 cells that had asymmetrically positioned spindles at anaphase onset.

Dynein activity is required for differential pole movement

To determine whether dynein activity contributes to differential pole movement in class III cells, we microinjected cells with the CC1 fragment of the p150 subunit of dynactin, an approach used effectively to interfere with the interaction between dynein and dynactin and to inhibit dynein-dependent processes in mammalian cells (Quintyne *et al.*, 1999; Gaetz and Kapoor, 2004; Ferenz and Wadsworth, 2007; Ma *et al.*, 2010). Cells with displaced spindles were microinjected with CC1 immediately after anaphase onset. The results showed that the differential movement of the leading pole was inhibited after microinjection of CC1 (Figure 4A, top), and the cleavage furrow was subsequently initiated away from the cell midpoint (Figure 4B). Control cells microinjected with buffer did not show displacement of the cleavage furrow (Figure 4A, bottom, and B). In addition, we observed that the spindle became disordered after microinjection of CC1, consistent with inhibition of dynein function (Gaetz and Kapoor, 2004). Similarly, we found that treatment of class III cells at the onset of anaphase with a low dose of nocodazole, 12.5 nM, which inhibits microtubule dynamics (Vasquez *et al.*, 1997), prevented the differential movement of the leading pole (Figure 4, C and D). These results demonstrate that dynein function and dynamic microtubules are required for differential pole motion during anaphase B.

Asymmetric cortical distribution of NuMA

We next examined the localization of NuMA, a member of the tripartite complex NuMA-LGN-Gαi, which is required for the cortical association of dynein (Du and Macara, 2004; Kiyomitsu and Cheeseman, 2012). LLC-Pk1 cells were double stained with antibodies against dynactin p150 and NuMA to compare the distributions of the two proteins at the cortex of mitotic cells (Figure 5A). We found that the distribution of NuMA was strikingly similar to that of p150, with both proteins either absent from the cortex or showing the same distribution (Figure 5B). For example, in metaphase cells with a centrally located spindle, NuMA and p150 were codistributed at both (57.6%) or one (36.4%) end in the majority of cells (Figure 5B, bottom). In metaphase cells with a displaced spindle, both proteins were localized at one end in >90% of cells (Figure 5B, bottom). A small percentage of cells (≤16% in all cases) exhibited different cortical distributions of the two proteins (Figure 5B, top, blue bars); of these, 85.7% showed that NuMA was present but p150 was absent, consistent with the role of NuMA as an upstream targeting factor of dynein/dynactin. The observed asymmetric distribution of cortical NuMA is distinct from the symmetric distribution observed in HeLa cells as previously reported (Kiyomitsu and Cheeseman, 2012; see *Discussion*).

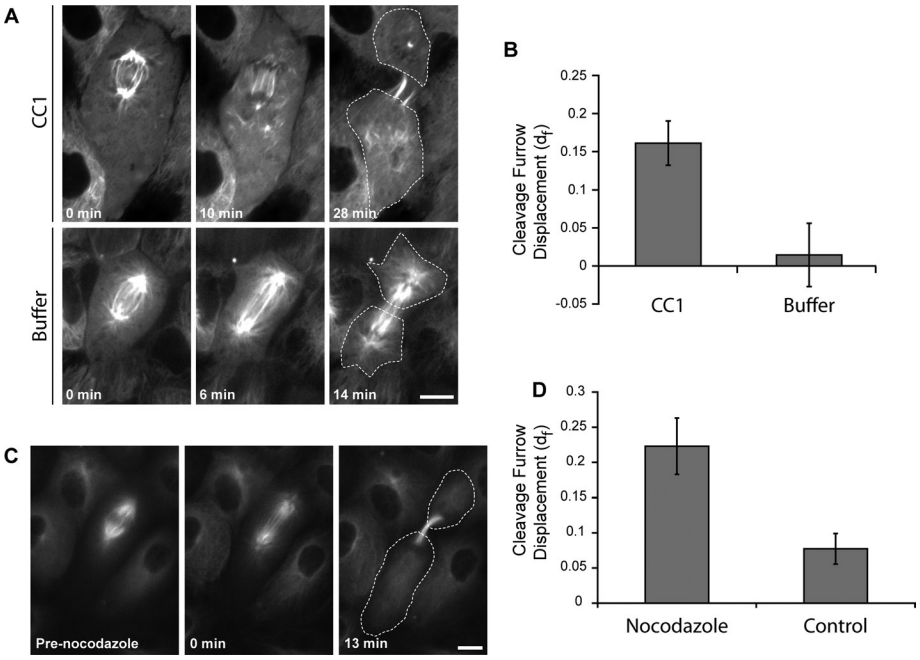

FIGURE 4: Dynein activity is required for leading pole motion. (A) Class III cells expressing GFP–α-tubulin were injected with CC1 to inhibit dynein and dynactin interaction (top) or injected with buffer (bottom). Cells were microinjected immediately before $t = 0$ min. Dashed line outlines the cell edge in the final frame. Scale bar, 10 μm. (B) Cleavage furrow displacement in CC1- and buffer-injected cells ($n = 10$ and 6 cells, respectively). Error bars represent SE of proportion. $p \leq 0.01$. (C) Time-lapse fluorescence images of an LLC-Pk1 cell expressing GFP–α-tubulin treated with 12.5 nM nocodazole. (D) Quantification of the cleavage furrow displacement in C for cells treated with 12.5 nM nocodazole or dimethyl sulfoxide control ($n = 10$ cells). $p \leq 0.01$.

Astral microtubules regulate accumulation of cortical dynein and dynactin

From our live-cell imaging, we observed that cortical enrichment of dynein and dynactin in metaphase cells was most pronounced in areas of the cortex that were furthest from the spindle, leading us to hypothesize that astral microtubules regulate the distribution of cortical dynein/dynactin. To test this hypothesis, we examined the distribution of microtubules and dynactin in fixed metaphase cells. We found that in cells with a displaced spindle, many astral microtubules reached the proximal cortex but few extended all the way to the distal cortex (Figure 6A, top). Similarly, we found that in metaphase cells that exhibited an irregular cell shape, cortical dynactin frequently accumulated as patches along membrane protrusions that were not directly accessible to astral microtubules (Figure 6A, middle). Conversely, among all of the cells that did not exhibit any detectable cortical dynactin staining, the spindle was generally positioned at the cell center, and astral microtubules extended to all regions of the cortex (unpublished data).

In anaphase cells, we noted that astral microtubules appeared longer than those in metaphase cells. We quantified the average

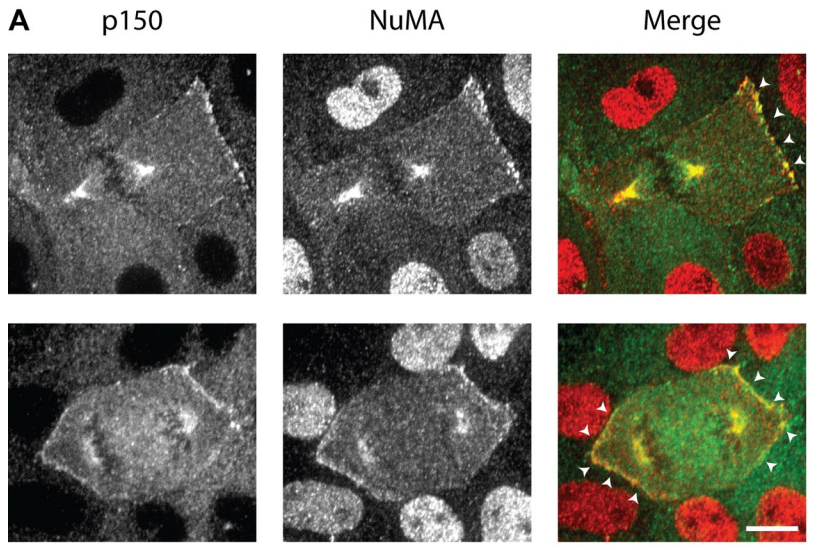

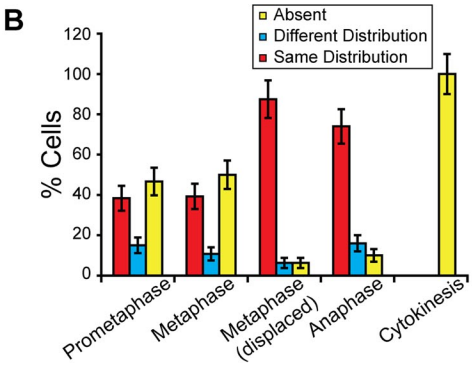

Same Distribution	One Side	Both Sides	Both Ends	One End
Prometaphase	19.6%	0%	45.7%	34.8%
Metaphase	6.1%	0%	57.6%	36.4%
Metaphase (displaced)	5.2%	0%	3.4%	91.4%
Anaphase	0.0%	2.8%	91.7%	5.6%

FIGURE 5: Codistribution of cortical NuMA and the p150 subunit of dynactin. (A) Immunofluorescence images of LLC-Pk1 cells stained with anti-p150 (left; green in merge) and anti-NuMA (middle; red in merge) antibodies; merged images to the right. Arrowheads, codistribution of NuMA and p150 at the cortex. Scale bar, 10 μm. (B) Top, quantitation of cortical NuMA and p150 distribution ($n = 231$ cells). Error bars represent SE of proportion. Bottom, patterns of NuMA and p150 codistribution observed in cells scored as same (red bars in B; $n = 121$ cells).

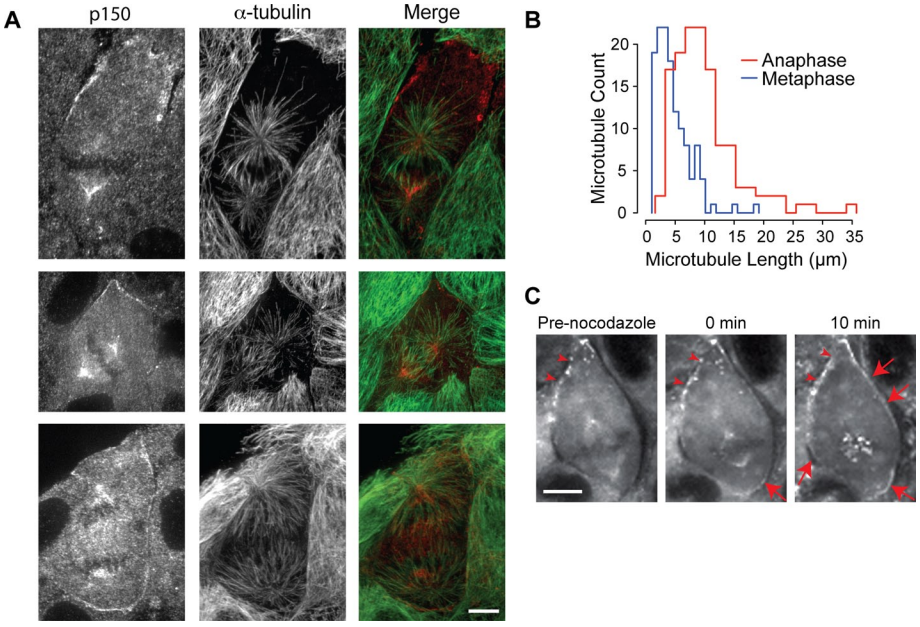

FIGURE 6: Dynein/dynactin accumulate at cortical sites distal to astral microtubules during metaphase. (A) Immunofluorescence images of LLC-Pk1 cells stained with anti-p150 antibodies (left; red in merge) and anti–α-tubulin (middle; green in merge) at metaphase with a displaced (top) or centered spindle (middle) and at anaphase with an elongated spindle and robust asters (bottom); merged images to the right. (B) Histograms of astral microtubule length during metaphase (blue) and anaphase (red; $n = 30$ cells; $p < 0.0001$). (C) Time-lapse fluorescence images of a metaphase cell expressing DHC-LAP treated with 33 μM nocodazole at $t = 0$ min. Arrowheads, preexisting cortical dynein patches; arrows, new dynein accumulation. Scale bars in A and C, 10 μm.

astral microtubule length by measuring the distance from the centrosome to the astral microtubule plus end and found that the average length increased significantly as cells progressed from metaphase to anaphase (Figure 6B). Significantly, in anaphase, we noted that many cells retained cortical dynactin, despite the presence of longer microtubules (Figure 6A, bottom). In summary, we found that in metaphase, dynein and dynactin are enriched in regions with few, and diminished in regions with many, astral microtubules; whereas in anaphase the effects of astral microtubules on cortical dynein/dynactin appear to be dampened.

To test our hypothesis that astral microtubules regulate cortical dynein in metaphase, we treated cells with nocodazole at concentrations that disassemble microtubules (Figure 6C; Jordan *et al.*, 1992) and monitored the distribution of cortical dynein. In five of eight nocodazole-treated metaphase cells, dynein was observed to appear at cortical regions previously devoid of detectable dynein (Figure 6C, red arrows). In addition, dynein and dynactin accumulated at kinetochores in nocodazole-treated cells. These results indicate that astral microtubules negatively regulate cortical dynein and dynactin.

Plk1 regulates accumulation of cortical dynein and dynactin

Plk1 has recently been shown to regulate the association of dynein with the cell cortex in HeLa cells (Kiyomitsu and Cheeseman, 2012). To examine the potential contribution of Plk1 to the cortical distribution of dynein and dynactin in LLC-Pk1 cells, we arrested cells in metaphase with MG132 and inhibited Plk1 activity with BI2536 (Figure 7, A and B). Addition of BI2536 resulted in an enhancement of cortical dynein fluorescence in 62.5% of cells ($n = 24$ cells). Most cells showed an increase in the fluorescence of existing cortical patches, as well as the appearance of dynein at cortical sites previously lacking detectable dynein (Figure 7A, arrowheads and arrows, respectively). In cells with a displaced spindle, the majority showed an increase in fluorescence of existing cortical dynein at the distal cortex; only a minority of cells showed new accumulations at the distal cortex (Figure 7B, Displaced (Distal); compare yellow and blue bars). In contrast, at the proximal cortex, we observed new accumulations of dynein, as well as increase in the fluorescence of existing cortical patches (Figure 7B, Displaced (Proximal)).

DISCUSSION

Cortical dynein and dynactin are dynamic and regulated by the cell cycle

Determining the dynamic localization of dynein and dynactin complexes in mammalian cells has been challenging due in part to the lack of suitable probes. Previous work using fixed cells demonstrated that dynein and dynactin localize to the mitotic cell cortex, appearing as a continuous cortical belt or in a patchy distribution (Busson *et al.*, 1998; Faulkner *et al.*, 2000). In live cells expressing GFP-tagged dynein IC, cortical dynein was detected, but its dynamics was not described (Kobayashi and Murayama, 2009). Recently, based on the use of LAP-tagged subunits of dynein and dynactin expressed from BACs, a dynamic cortical localization of dynein was reported (Kiyomitsu and Cheeseman, 2012). Consistent with this finding, we report dynamic cortical dynein and dynactin in LLC-Pk1 cells. We did not detect a continuous belt of dynein or dynactin as described. This discrepancy might result because the signal from the GFP tag on dynein or dynactin might be too weak to detect a low concentration of these complexes at the equatorial cortex. Alternatively, different cell types might have distinct distributions of dynein and dynactin.

The results of our experiments demonstrate that both dynein and dynactin dynamically associate with the mitotic cell cortex in mammalian cells. Using live-cell imaging, we show that in cells with a centrally located spindle, both complexes are detected at cortical regions distal to the spindle and are excluded from the equatorial region. In cells with asymmetrically localized spindles, dynein and dynactin were enriched at cortical regions distant from the spindle. The motion of the spindle within the cell was directed toward regions with enriched cortical dynein and dynactin, and both complexes were diminished after repositioning of the spindle in early mitosis. Because both dynein and dynactin subunits were tagged with GFP, we could not colocalize them in the same cell. However, both complexes exhibited a similar patch-like distribution in early mitosis and a more uniform distribution later in mitosis. Based on these observations, our data support the view that these complexes colocalize at the mitotic cortex in mammalian cells.

Our results demonstrate that the distribution of dynein and dynactin is regulated by the cell cycle. As mitosis progressed, the percentage of cells with detectable cortical dynein increased, with a peak in anaphase, and decreased as cells proceeded to cytokinesis. Enhanced cortical dynein and dynactin in anaphase could result

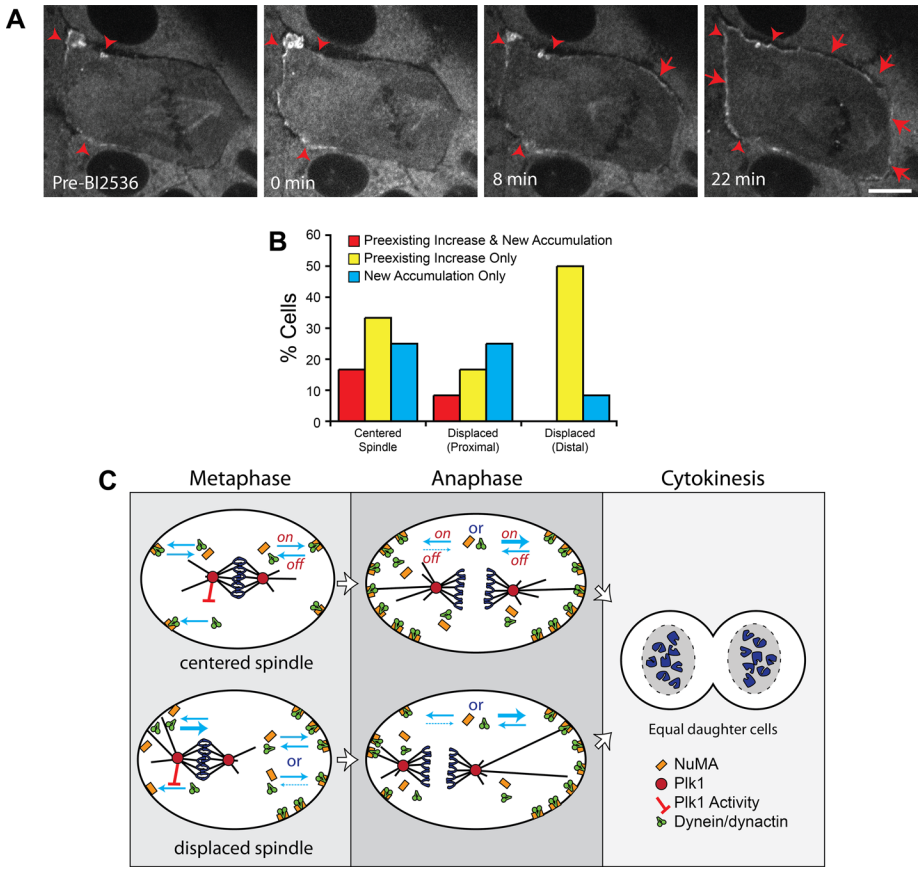

FIGURE 7: Inhibition of Plk1 kinase increases accumulation of cortical dynein. (A) Time-lapse fluorescence images of LLC-Pk1 cells expressing DHC-LAP arrested in metaphase with 5 μM MG132 and treated with 10 μM BI2536 at $t = 0$ min. Arrowheads, preexisting cortical dynein; arrows, new cortical dynein accumulation. Scale bar, 10 μm. (B) Quantitation of cortical dynein gain after BI2536 ($n = 24$ cells). (C) Model depicting cortical dynein in metaphase and anaphase cells. Top, centered spindles; bottom, displaced spindles. Plk1 inhibits the interaction between dynein/dynactin and cortical NuMA (red bar–headed line). Blue arrows represent on- and off-rates of dynein/dynactin and NuMA. In metaphase cells with a displaced spindle, the off-rate for dynein at the proximal cortex is increased (thick blue arrow). At the distal cortex, the on- and off-rates could be unchanged or the off-rate could be decreased relative to cells with a centered spindle. In anaphase, the on-rate is increased (thick blue arrow, right side) or, alternatively, the off-rate is decreased (dashed blue arrow, left side).

from increased association of the complexes at the cortex (higher on-rate), decreased dissociation (lower off-rate), or a combination of both (Figure 7C). Although cortical dynein and dynactin increased in anaphase, we noted that dynein at the cortex proximal to the aster was dimmer than that at the far cortex. Our results and those of Kiyomitsu and Cheeseman (2012) show that inhibition of Plk1 resulted in increased cortical dynein. One possibility is that astral microtubules convey an inhibitory spindle pole–derived Plk1 signal to the proximal cortex. The cell cycle regulation of cortical dynein and dynactin could result because signals from the spindle aster or pole change as cells progress through the cell cycle; alternatively, the association of dynein and dynactin with the cortex could be directly regulated by the cell cycle independently of astral microtubules.

Previous work showed that during early mitosis, dynein is responsible for the inward transport of peripheral microtubules to the spindle region (Rusan *et al.*, 2002), whereas during anaphase, microtubules move outward to repopulate the cell periphery (Rusan and Wadsworth, 2005). The cell cycle–dependent enrichment of cortical dynein and dynactin in anaphase could power the outward motion of microtubules and centrosome fragments in anaphase cells and the motion of spindle poles that we document here.

NuMA is dynamically localized to the cortex of LLC-Pk1 cells

Our observations of cortical dynein and dynactin dynamics are consistent with recent work using HeLa cells (Kiyomitsu and Cheeseman, 2012): in both cell types, the levels of cortical dynein and dynactin were reduced at the proximal and increased at the distal cortex; neither protein was detected at the equatorial region. In HeLa cells, the distribution of NuMA and LGN, members of the tripartite complex NuMA-LGN-Gαi, were distinct from that of dynein and dynactin, showing a symmetric distribution (Kiyomitsu and Cheeseman, 2012). In contrast, in LLC-Pk1 cells we found that the distribution of NuMA was asymmetric, suggesting that regulation of cortical dynein targeting in these cells is upstream of NuMA-LGN-Gαi complex. Consistent with this idea, inhibition of Plk1 in LLC-Pk1 cells did not result in a uniform cortical enhancement of dynein as observed in HeLa cells (Kiyomitsu and Cheeseman, 2012): cortical locations where dynein was present showed an enhancement of dynein, whereas regions lacking dynein were less likely to show a similar enhancement. This could result if cortical regions lacking dynein also lacked NuMA-LGN-Gαi, preventing the increase in dynein upon Plk1 inhibition. This finding indicates that the inhibitory effect of Plk1 on the recruitment of dynein to the cortex, as reported (Kiyomitsu and Cheeseman, 2012), acts at the level of the interaction between dynein/dynactin and the NuMA-LGN-Gαi complex (Figure 7C).

The spindle correction mechanism requires dynein and dynactin

Recent work has shown that artificial targeting of Gαi to the apical cortex resulted in spindle displacement in three-dimensional cultured Madin–Darby canine kidney (MDCK) cells (Xiao *et al.*, 2012). Anaphase spindle elongation was found to compensate for the spindle displacement, giving rise to equal-sized daughter cells. Our results show that in unperturbed LLC-Pk1 cells, mitotic spindles frequently moved along the long axis of the cell and as a result were frequently mispositioned at anaphase onset. In these cells, we found that differential pole motion during anaphase onset results in the formation of equal-sized daughter cells. Our results further show that dynein and dynactin and dynamic astral microtubules are required to correct spindle displacement. Although previous studies showed that NRK cells delay the onset of anaphase upon externally induced spindle misalignment (O'Connell and Wang, 2000), we did not detect any delay in the onset of anaphase for LLC-Pk1 cells exhibiting a displaced spindle, suggesting that there might be an inherent difference in the surveillance mechanism between the two

cell lines. Typically, asymmetric cell division results from a displaced spindle (Siller and Doe, 2009; Gillies and Cabernard, 2011; Morin and Bellaiche, 2011), suggesting that distinct cell types might override the correction mechanism so as to generate unequal-sized daughter cells.

The dynamic and cell cycle–regulated distribution of dynein and dynactin that we report here are consistent with the following model for spindle positioning. During early mitosis, astral microtubules interact with dynein and dynactin at the cell cortex; an imbalance of forces on the asters results in motion of the spindle toward cortical regions of higher dynein density (Grill *et al.*, 2001, 2003). Spindles were often observed to reside near the cortex for several minutes, suggesting that residual dynein and dynactin might tether the spindle to the cortex (Laan *et al.*, 2012). With time, cortical dynein was reduced in regions near astral microtubules. This could result if dynein and dynactin are removed from the cortex by walking toward the microtubule minus end. One possibility is that NuMA is removed from the cortex as a cargo of dynein (Merdes *et al.*, 2000). Alternatively, dynein and dynactin could be released from the cortex directly to the cytoplasm (Figure 7C). At cortical regions distant from the aster and pole, dynein and dynactin accumulate; stochastic interactions of astral microtubules with these regions can result in repositioning of the metaphase spindle within the cell, concomitant with removal of dynein, potentially resulting in multiple motions of the spindle within the cell.

We propose that differential spindle pole motion in anaphase results from dynamic astral microtubules extending to the distal polar cortex, where they engage cortical dynein and dynactin. Our model predicts that the change in microtubule dynamics at the metaphase–anaphase transition (Rusan *et al.*, 2001) and the observed enhancement of dynein and dynactin at the anaphase cortex would increase the probability of a dynamic microtubule encountering cortical dynein/dynactin. Furthermore, as previously proposed (O'Connell and Wang, 2000; Tolic-Norrelykke, 2010), longer astral microtubules might associate with a greater number of motors, and thus it is conceivable that astral microtubules extending from the leading pole might experience a higher pulling force that results in moving the displaced spindle. Although we did not detect dynein or dynactin at the dorsal or ventral cortex, recent work demonstrated that motors in the cytoplasm can generate forces and could contribute to spindle positioning (Kimura and Kimura, 2011; Wuhr *et al.*, 2010).

In summary, we provide evidence for dynamic cortical association of dynein and dynactin in mammalian cells and its regulation by Plk1, astral microtubules, and the cell cycle. The asymmetric spindle positioning in LLC-Pk1 cells and its correction by dynein and dynactin provide a new system for analysis of spindle position and symmetric cell division.

MATERIALS AND METHODS

Cell culture

LLC-Pk1 cells expressing GFP–α-tubulin (LLC-Pk1-α), DHC-LAP, or p50-LAP were cultured in a 1:1 mixture of Opti-MEM and F-10 media supplemented with 7.5% fetal bovine serum and antibiotics. Cells were grown in a 5% CO_2 atmosphere at 37°C. For time-lapse imaging experiments, cells were plated onto glass coverslips 48–72 h before imaging.

Immunofluorescence

Cells were rinsed in 37°C phosphate-buffered saline (PBS) and fixed in either –20°C methanol or 3.2% paraformaldehyde, 0.1% glutaraldehyde, and 0.05% Triton in PBS at 37°C for 20 min, followed by postfixation in methanol at –20°C for 6 min, and rehydrated in PBS containing 0.1% Tween-20 and 0.02% sodium azide (PBS-Tw-Az) for 5 min at room temperature. Cells were then blocked with 3% bovine serum albumin and 0.5% Tween in PBS-Tw-Az for 1 h at room temperature. Primary antibody staining was performed with anti-p150 at 1:100 (BD Transduction Laboratories, Lexington, KY), anti-tubulin at 1:100 (Accurate Chemical and Scientific Corporation, Westbury, NY), or anti-NuMA at 1:5000 (a kind gift from Duane Compton, Dartmouth College, Hanover, NH) for 1 h at room temperature. Secondary antibody staining was performed with Cy3-labeled anti-mouse antibodies at 1:400 (Jackson ImmunoResearch Laboratories, West Grove, PA) or fluorescein isothiocyanate–labeled anti-rat antibodies at 1:128 (Sigma-Aldrich, St. Louis, MO) for 8 h at 4°C. Coverslips were mounted in Vectashield (Vector Laboratories, Burlingame, CA) and sealed with nail polish.

Inhibitors

For metaphase arrest, LLC-Pk1 cells were incubated for 1 h with 5 μM MG132 before imaging. For Plk1 inhibition, cells were treated with 10 μM BI2536. Nocodazole was used at 12.5 nM to inhibit microtubule dynamics or at 16 or 33 μM to disassemble microtubules.

BAC cell line generation and characterization

The DHC and p50 subunits were labeled at the C-terminus with a LAP tag (Poser *et al.*, 2008). The LAP tag comprises an S-peptide tag and a GFP tag at the C-terminus of the target protein (Cheeseman and Desai, 2005). Mouse DHC and p50 BACs were kind gifts from Anthony Hyman (European Molecular Biology Laboratory, Heidelberg, Germany). Bacteria containing the BAC were grown on LB plates conditioned with chloramphenicol. Subsequent cloning steps to insert the LAP tag were performed according to Gene Bridges-Counter Selection BAC Modification Kit, version 3.1 (Gene Bridges, Heidelberg, Germany). Bacteria were prepared for electroporation at 4°C and electroporated at 1.8 kV. The LAP-tagged BAC was purified using Nucleobond BAC 100 Maxi Prep protocol (Clontech, Mountain View, CA).

To create the p50-LAP cell line, we plated LLC-Pk1 cells at a density of 1.0×10^5 and transfected them 48 h later with LAP-tagged BAC using an Amaxa Nucleofector according to the protocol recommended by the manufacturer (Lonza, Walkersville, MD). To create the DHC-LAP cell line, we plated LLC-Pk1 cells to a density of 2.0×10^5 and transfected them 24 h later using Effectene Transfection Reagent according to the protocol recommended by the manufacturer (Qiagen, Valencia, CA). Cells were selected in 400 μg/ml G418 for 2 wk. Cell lines stably expressing LAP-tagged p50 and DHC were prepared using established protocols (Wadsworth *et al.*, 2005).

Preparation of whole-cell extracts and pull down with S-agarose beads

LLC-Pk1 cells expressing p50-LAP and DHC-LAP were treated with 100 nM nocodazole 20 h before preparation of cell extracts. Cells were lysed in 50 mM 4-(2-hydroxyethyl)-1-piperazineethanesulfonic acid, 150 mM NaCl, 1% NP-40, and protease inhibitors (0.04 mg/ml aprotinin, 0.02 μg/ml leupeptin, and 0.2 mg/ml Pefabloc). Lysates were incubated on ice for 10 min with agitation every 5 min and spun at 14,100 × *g* in a microcentrifuge for 30 min at 4°C. S-agarose beads were washed with lysis buffer, and the lysate was added to the washed S-agarose beads. The mixture was incubated for 1 h at 4°C with rotation. After incubation, the beads were spun down and washed with lysis buffer. Beads with bound proteins were resuspended in SDS sample buffer and boiled for 3 min before SDS–PAGE.

Western blotting and detection

Protein samples were run on a 10% polyacrylamide gel and transferred onto Amersham Hybond-P membrane (GE Healthcare, Waukesha, WI). Blots were probed with mouse anti-p150 antibody (used at 1:1000; BD Transduction Laboratories), mouse 74.1 anti-dynein IC antibody (used at 1:1000; Chemicon, Temecula, CA,), or mouse anti-p50 antibody (used at 1:1000; BD Transduction Laboratories) for 1 h at room temperature in 5% nonfat dry milk dissolved in Tris-buffered saline containing 0.02% Tween-20 (TBS-Tween). The blots were then probed with goat anti-mouse horseradish peroxidase–conjugated secondary antibody (1:5000) for 1 h at room temperature in 5% nonfat dry milk dissolved in TBS-Tween and were detected using chemiluminescence.

Microinjection

To inhibit dynein function, we injected the CC1 fragment of p150 (Ferenz and Wadsworth, 2007) at 15 μM in 50 mM potassium glutamate and 1 mM $MgCl_2$, pH 7.0, containing 1 mg/ml 10-kDa rhodamine-labeled dextran (Molecular Probes, Eugene, OR) in order to track the microinjected cell.

Image acquisition and analysis

We acquired images using spinning disk confocal microscopy. We used two different microscopes: an Eclipse TE300 microscope (Nikon, Melville, NY) equipped with a CSU 10 spinning disk confocal scan head (PerkinElmer, Wellesley, MA) and an Orca-ER cooled charge-coupled device (CCD) camera (Hamamatsu, Bridgewater, NJ), or a Nikon TiE microscope with a CSU-x1 Yokogawa spinning disk confocal scan head (PerkinElmer) and an Andor iXon+ electron-multiplying CCD camera (Andor, Belfast, Northern Ireland). Both microscope systems were controlled by MetaMorph software (Molecular Devices, Sunnyvale, CA). We used a 100×/numerical aperture (NA) 1.4 objective for fluorescence imaging and a 20×/NA 0.5 objective for phase contrast imaging. For live-cell imaging, exposures were adjusted without saturating the camera's pixels; typical exposures were 50–1000 ms. For total internal reflection fluorescence microscopy we used a customized system exactly as described previously (Gable *et al.*, 2012). For drug treatments, cells in Rose chambers were imaged, and then nocodazole at 16 or 33 μM (to dissemble microtubules), nocodazole at 12.5 nM (to inhibit microtubules dynamics), or BI2536 at 5 μM (to inhibit Plk1 activity) in non-CO_2 tissue culture medium was added to the dish. Then the top of the chamber was replaced, and imaging resumed. Cells were maintained at ~37°C during the experiment, but the heater was turned off during changing of the medium. We measured the spindle displacement along the long axis of the cell at anaphase onset as [0.5 × cell length − (distance between chromosome bundle and the proximal cortex)]/(0.5 × cell length). Similarly, the displacement of the cleavage furrow was calculated as (distance between the cleavage furrow and the proximal cortex)/(0.5 × cell length). Spindle pole velocity was calculated from kymographs generated from time-lapse phase contrast images using chromosome bundles as reference point. Intensity measurements, daughter cell area measurements, and kymograph constructions were performed using ImageJ software (National Institutes of Health, Bethesda, MD). For cells treated with BI2536 or nocodazole, increase in preexisting dynein intensity was measured using movie frames from pretreatment and ~30 min after treatment; an increase in intensity of 10% or greater was scored as positive. New accumulations of dynein at the cortex were visually scored by two independent observers. To determine statistical significance, Student's *t* test was performed.

ACKNOWLEDGMENTS

We thank I. Poser and A. Hyman for generously providing the LAP-tagged dynein and dynactin BAC constructs and for advice with BAC cloning and Duane Compton for the NuMA antibodies. We thank Kaitlin Brooke for contributing greatly to the initial stages of this work. We thank Janel Titus for critically reading the manuscript, Carey Fagerstrom for technical assistance, and Vivienne Collins for her continued cooperation. This work was supported by a National Institutes of Health grant to W.L.L. (R01GM076094), a National Science Foundation award to P.W. (DBI-0923318), and a National Research Service Awards postdoctoral fellowship (F32GM093602) to E.S.C.

REFERENCES

Bruning-Richardson A, Langford KJ, Ruane P, Lee T, Askham JM, Morrison EE (2011). EB1 is required for spindle symmetry in mammalian mitosis. PLoS One 6, e28884.

Burkhardt JK, Echeverri CJ, Nilsson T, Vallee RB (1997). Overexpression of the dynamitin (p50) subunit of the dynactin complex disrupts dynein-dependent maintenance of membrane organelle distribution. J Cell Biol 139, 469–484.

Busson S, Dujardin D, Moreau A, Dompierre J, De Mey JR (1998). Dynein and dynactin are localized to astral microtubules and at cortical sites in mitotic epithelial cells. Curr Biol 8, 541–544.

Carminati JL, Stearns T (1997). Microtubules orient the mitotic spindle in yeast through dynein-dependent interactions with the cell cortex. J Cell Biol 138, 629–641.

Cheeseman IM, Desai A (2005). A combined approach for the localization and tandem affinity purification of protein complexes from metazoans. Sci STKE 2005, pl1.

Couwenbergs C, Labbe JC, Goulding M, Marty T, Bowerman B, Gotta M (2007). Heterotrimeric G protein signaling functions with dynein to promote spindle positioning in *C. elegans*. J Cell Biol 179, 15–22.

Cowan CR, Hyman AA (2004). Asymmetric cell division in *C. elegans*: cortical polarity and spindle positioning. Annu Rev Cell Dev Biol 20, 427–453.

Du Q, Macara IG (2004). Mammalian Pins is a conformational switch that links NuMA to heterotrimeric G proteins. Cell 119, 503–516.

Du Q, Taylor L, Compton DA, Macara IG (2002). LGN blocks the ability of NuMA to bind and stabilize microtubules. A mechanism for mitotic spindle assembly regulation. Curr Biol 12, 1928–1933.

Dujardin DL, Vallee RB (2002). Dynein at the cortex. Curr Opin Cell Biol 14, 44–49.

Echeverri CJ, Paschal BM, Vaughan KT, Vallee RB (1996). Molecular characterization of the 50-kD subunit of dynactin reveals function for the complex in chromosome alignment and spindle organization during mitosis. J Cell Biol 132, 617–633.

Faulkner NE, Dujardin DL, Tai CY, Vaughan KT, O'Connell CB, Wang Y, Vallee RB (2000). A role for the lissencephaly gene LIS1 in mitosis and cytoplasmic dynein function. Nat Cell Biol 2, 784–791.

Ferenz NP, Wadsworth P (2007). Prophase microtubule arrays undergo flux-like behavior in mammalian cells. Mol Biol Cell 18, 3993–4002.

Gable A *et al.* (2012). Dynamic reorganization of Eg5 in the mammalian spindle throughout mitosis requires dynein and TPX2. Mol Biol Cell 23, 1254–1266.

Gaetz J, Kapoor TM (2004). Dynein/dynactin regulate metaphase spindle length by targeting depolymerizing activities to spindle poles. J Cell Biol 166, 465–471.

Gillies TE, Cabernard C (2011). Cell division orientation in animals. Curr Biol 21, R599–R609.

Grill SW, Gonczy P, Stelzer EH, Hyman AA (2001). Polarity controls forces governing asymmetric spindle positioning in the *Caenorhabditis elegans* embryo. Nature 409, 630–633.

Grill SW, Howard J, Schaffer E, Stelzer EH, Hyman AA (2003). The distribution of active force generators controls mitotic spindle position. Science 301, 518–521.

Jordan MA, Thrower D, Wilson L (1992). Effects of vinblastine, podophyllotoxin and nocodazole on mitotic spindles. Implications for the role of microtubule dynamics in mitosis. J Cell Sci 102, Pt 3, 401–416.

Kimura K, Kimura A (2011). Intracellular organelles mediate cytoplasmic pulling force for centrosome centration in the *Caenorhabditis elegans* early embryo. Proc Natl Acad Sci USA 108, 137–142.

Kiyomitsu T, Cheeseman IM (2012). Chromosome- and spindle-pole-derived signals generate an intrinsic code for spindle position and orientation. Nat Cell Biol 14, 311–317.
Knoblich JA (2010). Asymmetric cell division: recent developments and their implications for tumour biology. Nat Rev Mol Cell Biol 11, 849–860.
Kobayashi T, Murayama T (2009). Cell cycle-dependent microtubule-based dynamic transport of cytoplasmic dynein in mammalian cells. PLoS One 4, e7827.
Krueger LE, Wu JC, Tsou MF, Rose LS (2010). LET-99 inhibits lateral posterior pulling forces during asymmetric spindle elongation in *C. elegans* embryos. J Cell Biol 189, 481–495.
Laan L, Pavin N, Husson J, Romet-Lemonne G, van Duijn M, Lopez MP, Vale RD, Julicher F, Reck-Peterson SL, Dogterom M (2012). Cortical dynein controls microtubule dynamics to generate pulling forces that position microtubule asters. Cell 148, 502–514.
Labbe JC, McCarthy EK, Goldstein B (2004). The forces that position a mitotic spindle asymmetrically are tethered until after the time of spindle assembly. J Cell Biol 167, 245–256.
LaMonte BH, Wallace KE, Holloway BA, Shelly SS, Ascano J, Tokito M, Van Winkle T, Howland DS, Holzbaur EL (2002). Disruption of dynein/dynactin inhibits axonal transport in motor neurons causing late-onset progressive degeneration. Neuron 34, 715–727.
Ligon LA, Karki S, Tokito M, Holzbaur EL (2001). Dynein binds to beta-catenin and may tether microtubules at adherens junctions. Nat Cell Biol 3, 913–917.
Ma N, Tulu US, Ferenz NP, Fagerstrom C, Wilde A, Wadsworth P (2010). Poleward transport of TPX2 in the mammalian mitotic spindle requires dynein, Eg5, and microtubule flux. Mol Biol Cell 21, 979–988.
Markus SM, Lee WL (2011). Regulated offloading of cytoplasmic dynein from microtubule plus ends to the cortex. Dev Cell 20, 639–651.
Markus SM, Punch JJ, Lee WL (2009). Motor- and tail-dependent targeting of dynein to microtubule plus ends and the cell cortex. Curr Biol 19, 196–205.
McCarthy EK, Goldstein B (2006). Asymmetric spindle positioning. Curr Opin Cell Biol 18, 79–85.
Merdes A, Heald R, Samejima K, Earnshaw WC, Cleveland DW (2000). Formation of spindle poles by dynein/dynactin-dependent transport of NuMA. J Cell Biol 149, 851–862.
Merdes A, Ramyar K, Vechio JD, Cleveland DW (1996). A complex of NuMA and cytoplasmic dynein is essential for mitotic spindle assembly. Cell 87, 447–458.
Morin X, Bellaiche Y (2011). Mitotic spindle orientation in asymmetric and symmetric cell divisions during animal development. Dev Cell 21, 102–119.
Morrison SJ, Kimble J (2006). Asymmetric and symmetric stem-cell divisions in development and cancer. Nature 441, 1068–1074.
Nguyen-Ngoc T, Afshar K, Gonczy P (2007). Coupling of cortical dynein and G alpha proteins mediates spindle positioning in *Caenorhabditis elegans*. Nat Cell Biol 9, 1294–1302.
O'Connell CB, Wang YL (2000). Mammalian spindle orientation and position respond to changes in cell shape in a dynein-dependent fashion. Mol Biol Cell 11, 1765–1774.
Poser I *et al*. (2008). BAC TransgeneOmics: a high-throughput method for exploration of protein function in mammals. Nat Methods 5, 409–415.
Quintyne NJ, Gill SR, Eckley DM, Crego CL, Compton DA, Schroer TA (1999). Dynactin is required for microtubule anchoring at centrosomes. J Cell Biol 147, 321–334.
Rankin KE, Wordeman L (2010). Long astral microtubules uncouple mitotic spindles from the cytokinetic furrow. J Cell Biol 190, 35–43.
Rappaport R (1996). Cytokinesis in Animal Cells, Cambridge: Cambridge University Press.
Rusan NM, Fagerstrom CJ, Yvon AM, Wadsworth P (2001). Cell cycle-dependent changes in microtubule dynamics in living cells expressing green fluorescent protein-alpha tubulin. Mol Biol Cell 12, 971–980.
Rusan NM, Tulu US, Fagerstrom C, Wadsworth P (2002). Reorganization of the microtubule array in prophase/prometaphase requires cytoplasmic dynein-dependent microtubule transport. J Cell Biol 158, 997–1003.
Rusan NM, Wadsworth P (2005). Centrosome fragments and microtubules are transported asymmetrically away from division plane in anaphase. J Cell Biol 168, 21–28.
Samora CP, Mogessie B, Conway L, Ross JL, Straube A, McAinsh AD (2011). MAP4 and CLASP1 operate as a safety mechanism to maintain a stable spindle position in mitosis. Nat Cell Biol 13, 1040–1050.
Schneider SQ, Bowerman B (2003). Cell polarity and the cytoskeleton in the *Caenorhabditis elegans* zygote. Annu Rev Genet 37, 221–249.
Siller KH, Doe CQ (2008). Lis1/dynactin regulates metaphase spindle orientation in *Drosophila* neuroblasts. Dev Biol 319, 1–9.
Siller KH, Doe CQ (2009). Spindle orientation during asymmetric cell division. Nat Cell Biol 11, 365–374.
Siller KH, Serr M, Steward R, Hays TS, Doe CQ (2005). Live imaging of *Drosophila* brain neuroblasts reveals a role for Lis1/dynactin in spindle assembly and mitotic checkpoint control. Mol Biol Cell 16, 5127–5140.
Tolic-Norrelykke IM (2010). Force and length regulation in the microtubule cytoskeleton: lessons from fission yeast. Curr Opin Cell Biol 22, 21–28.
Vasquez RJ, Howell B, Yvon AM, Wadsworth P, Cassimeris L (1997). Nanomolar concentrations of nocodazole alter microtubule dynamic instability in vivo and in vitro. Mol Biol Cell 8, 973–985.
Wadsworth P, Rusan NM, Tulu US, Fagerstrom C (2005). Stable expression of fluorescently tagged proteins for studies of mitosis in mammalian cells. Nat Methods 2, 981–987.
Woodard GE, Huang NN, Cho H, Miki T, Tall GG, Kehrl JH (2010). Ric-8A and Gi alpha recruit LGN, NuMA, and dynein to the cell cortex to help orient the mitotic spindle. Mol Cell Biol 30, 3519–3530.
Wuhr M, Tan ES, Parker SK, Detrich HW 3rd, Mitchison TJ (2010). A model for cleavage plane determination in early amphibian and fish embryos. Curr Biol 20, 2040–2045.
Xiao Z, Wan Q, Du Q, Zheng Z (2012). Galpha/LGN-mediated asymmetric spindle positioning does not lead to unequal cleavage of the mother cell in 3-D cultured MDCK cells. Biochem Biophys Res Commun 420, 888–894.